

Article

Hydrogen-Rich Gas Production with the Ni-La/Al₂O₃-CaO-C Catalyst from Co-Pyrolysis of Straw and Polyethylene

Jianfen Li ^{1,*}, Rongyi Gao ¹, Longkai Zhu ¹, Yiran Zhang ¹, Zeshan Li ¹, Bolin Li ¹, Jiayang Wang ¹, Ji He ¹, Yun He ¹, Zhenhua Qin ¹, Mahmood Laghari ² and Dabin Guo ^{3,*}

¹ School of Chemical and Environmental Engineering, Wuhan Polytechnic University, Wuhan 430023, China; gry9706@126.com (R.G.); zlk1044534634@163.com (L.Z.); zhangyr2022@126.com (Y.Z.); leezees@163.com (Z.L.); bolinli97@163.com (B.L.); vlp110@163.com (J.W.); hj4349@126.com (J.H.); yunhe7@whpu.edu.cn (Y.H.); whpuchem@126.com (Z.Q.)

² Department of Energy and Environment, Sindh Agriculture University, Tandojam 70060, Pakistan; mlaghari@sau.edu.pk

³ School of Civil Engineering, Guangzhou University, Guangzhou 510006, China

* Correspondence: whpulijfen@126.com (J.L.); dabin@gzhu.edu.cn (D.G.)

Abstract: Ni-based catalysts have been extensively investigated because of their superior catalytic performance. In this study, the Ni-La/Al₂O₃-CaO-C catalyst was prepared by homogeneous precipitation, employed in the co-pyrolysis of soybean straw with polyethylene to produce hydrogen. The optimal experimental conditions were identified by discussing the carrier synthesis ratio, feedstock ratio, and addition of La. Additionally, the stability of the catalyst was evaluated. It was established that the carrier was produced using a molar ratio, the raw ingredients ratio of 5:5, and that the optimum catalytic action was obtained when La was added. Co-pyrolysis of soybean straw with polyethylene (PE) that was catalyzed by Ni-La/Al₂O₃-CaO-C generated 55.45 vol% of H₂ under ideal experimental circumstances. After six applications, the H₂ yield was 33.89 vol%, compared to 27.5 vol% for the Ni/Al₂O₃-CaO-C catalyst. The experimental results indicate that Ni-La/Al₂O₃-CaO-C exhibits superior catalytic activity and stability than Ni/Al₂O₃-CaO-C.

Keywords: co-pyrolysis; Ni-based catalyst; Ni-La; hydrogen; straw; polyethylene



Citation: Li, J.; Gao, R.; Zhu, L.; Zhang, Y.; Li, Z.; Li, B.; Wang, J.; He, J.; He, Y.; Qin, Z.; et al.

Hydrogen-Rich Gas Production with the Ni-La/Al₂O₃-CaO-C Catalyst from Co-Pyrolysis of Straw and Polyethylene. *Catalysts* **2022**, *12*, 496. <https://doi.org/10.3390/catal12050496>

Academic Editor: Yu-Chuan Lin

Received: 25 March 2022

Accepted: 22 April 2022

Published: 28 April 2022

Publisher's Note: MDPI stays neutral with regard to jurisdictional claims in published maps and institutional affiliations.



Copyright: © 2022 by the authors. Licensee MDPI, Basel, Switzerland. This article is an open access article distributed under the terms and conditions of the Creative Commons Attribution (CC BY) license (<https://creativecommons.org/licenses/by/4.0/>).

1. Introduction

Energy demand is increasing day by day with the development of society. According to BP Amoco's statistical review in Figure 1, energy consumption in the world reached 556.63 exajoules in 2020. Fossil fuel consumption accounts for 83.13% of the global total energy consumption. By contrast, renewable energy consumption accounts for only 5.70% [1]. Long-term reliance on fossil fuels has devastated our ecosystem, causing the greenhouse effect, ozone layer depletion, and acid rain [2]. Simultaneously, increased usage of fossil fuels will precipitate an energy catastrophe. As a result, it is essential for us to use more renewable energy and less fossil fuels.

Renewable energy sources are plentiful and diverse, including solar energy, wind energy, biomass, etc. Biomass is a low-cost and renewable resource composed mostly of cellulose, hemicellulose, and lignin, but the proportions of these components vary according to the kind of biomass [3]. Biomass is primarily converted to energy via two processes: thermochemical and biochemical conversion. Thermochemical conversion of biomass primarily consists of the following: combustion, gasification, liquefaction, and pyrolysis [4–7]. Among the several thermochemical conversion processes, pyrolysis is considered one of the most promising due to its high carbon neutralization ability [8,9].

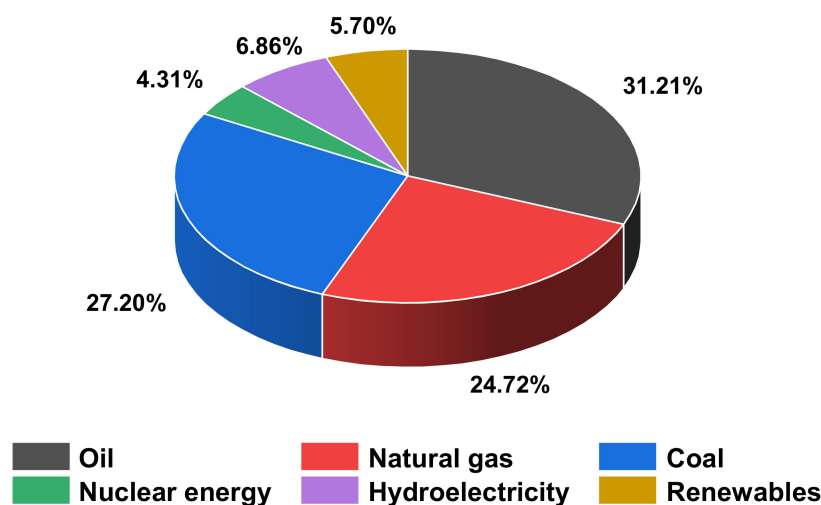


Figure 1. Primary energy: consumption by fuel.

To better understand the co-pyrolysis of rice straw (RS) and polyethylene (PE), Kai et al. [10] used TG-FTIR-MS to analyze the co-pyrolysis process. The results indicated that RS co-pyrolysis with high density polyethylene (HDPE) could be split into two stages: RS pyrolysis and HDPE pyrolysis, and the two interacted considerably between 435–520 °C. Fan et al. [11] discovered that when RS and PE were co-pyrolyzed, no new material was formed, and the inclusion of PE assisted in the degradation of RS. Yang et al. [12] co-gasified rice straw with PE, polyvinyl chloride (PVC), and polyethylene terephthalate (PET); and, they found that the activation energy required to co-gasify rice straw with PE and PVC is less than the weighted sum of the individual activation energies of the substances, indicating that rice straw gasification with PE and PVC has a synergistic effect. Sajdak's [13] study demonstrated that the inclusion of multicomponent plastics had the most significant influence on gaseous and liquid yields during biomass pyrolysis.

The output of gas from single biomass pyrolysis is restricted. However, by adding PE to the biomass pyrolysis process, the yield of H₂ may be efficiently increased. Zhang et al. [14] synthesized hydrogen-rich gas using a Ni-Fe@nanofibers/porous carbon catalyst. The maximum hydrogen generation rate of 33.66 mmol/g was achieved using pyrolysis-gasification of biomass and waste plastics at a biomass to plastic ratio of 1:2 and a gasification temperature of 700 °C. Chai et al. [15] prepared Ni-CaO-C catalysts for the co-pyrolysis of pine wood chips and HDPE, polypropylene (PP), and polystyrene (PS) for hydrogen production. The results indicated that the greatest outcomes were obtained with a biomass to plastic ratio of 7:3. Of the three polymers, HDPE had the most excellent H₂ output, with 80.36 mmol/g at 700 °C and a 5 mL/h water injection rate. Finally, there is a synergistic impact on producing H₂ when combined with biomass and waste plastics.

Additionally, the catalyst is a crucial influencing aspect. Due to their superior catalytic performance, Ni-based catalysts were extensively explored in the past [16]. However, Ni-based catalysts are prone to deactivation. This is mostly due to the reduction in the specific surface area of the catalyst caused by metal particle sintering: coke obstructing the active center and preventing the metal particles from interacting with the carrier [17,18]. So, improving the service life of Ni-based catalysts remains a pressing issue.

Currently, co-pyrolysis is being explored mostly for the purpose of pyrolysis oil production and comparatively little H₂ production. Because of its large volatile percentage (>80%), soybean straw was used as a feedstock for catalytic pyrolysis in this investigation. Due to its superior catalytic activity and cheap cost, Ni was chosen as the active component [19]; and, the addition of La further increased the catalytic activity and stability. Using activated carbon and metal composites as a carrier, Ni-La/Al₂O₃-CaO-C (ACC) catalyst was made. The impact of the catalyst on hydrogen generation by co-pyrolysis in

soybean straw and PE was evaluated by adjusting the ratio of carrier synthesis, the ratio of co-pyrolysis feedstocks, and the number of times the catalyst was applied.

2. Results and Discussion

2.1. Characterization of Catalysts

The catalysts were analyzed by XRD, XRF, BET, and SEM-EDS.

The XRD analysis in Figure 2 observed the characteristic peaks of mayenite ($\text{Ca}_{12}\text{Al}_{14}\text{O}_{33}$), suggesting a good stability of the catalysts [20,21]. The NiO and the La_2O_3 phases were seen in the fresh catalysts, showing that the active components are mainly in the form of oxides. However, the Ni species were discovered in used catalysts. This may be because NiO was reduced to Ni by reducing gas in a high temperature environment, and then it participated in the pyrolysis process as Ni. Moreover, after adding La to the Ni/ACC(M) catalyst, the intensity of the NiO diffraction peak was reduced [22]. One of the most noticeable differences between fresh and used catalysts is that the NiCx diffraction peaks grow sharper, suggesting a large NiCx crystal size. Furthermore, adding La significantly reduced the sharpness of NiCx peaks, showing the small crystal size of NiCx.

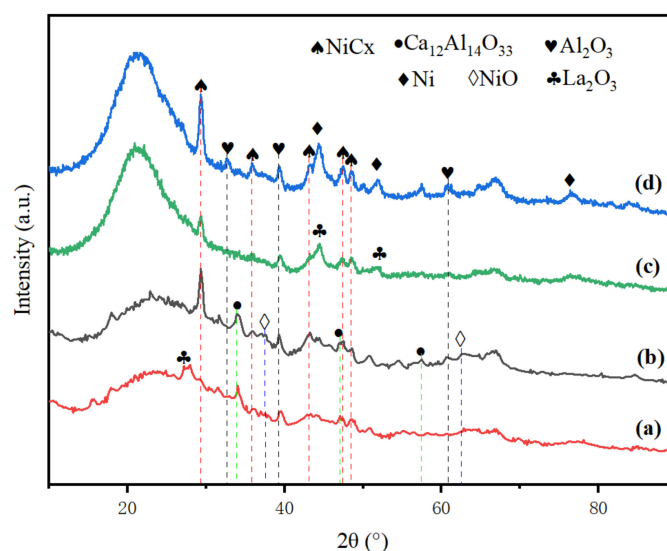


Figure 2. XRD patterns for catalysts: (a) fresh Ni-La/ACC(M); (b) fresh Ni/ACC(M); (c) used Ni-La/ACC(M); (d) used Ni/ACC(M).

Table 1 presents the XRF analysis of supports and catalysts loaded with active metals. The main components in the carriers are metal oxides. As for synthesized ACC(W), the mass ratio of Al_2O_3 and CaO is nearly 1:1. Additionally, the Al_2O_3 to CaO mass ratio in ACC(M) is 1.90, which is close to the theoretical calculation value of 1.82. The above data demonstrate that the carrier synthesis is mostly compatible with the computation. It is clear that the active components of Ni and of La both reached over the design loads of 10 wt%, indicating that the catalysts were synthesized successfully. There are some differences between the design loads and the actual loads, owing to the unstable hydration state of starting salts [23].

Table 1. XRF analysis of supports and catalysts.

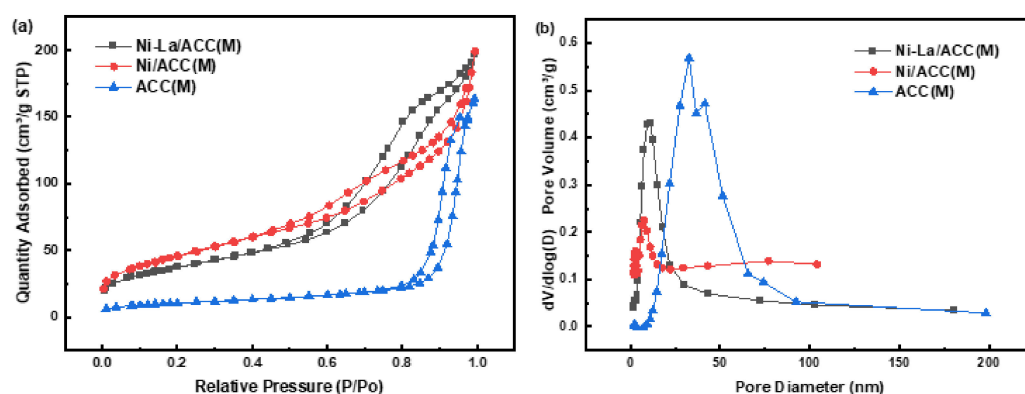
Samples	Main Composition and Content (wt%)				
	Al ₂ O ₃	CaO	NiO	La ₂ O ₃	Others
ACC(W)	46.52	51.16	-	-	2.32
ACC(M)	63.73	33.52	-	-	2.75
Ni/ACC(M)	56.95	28.01	12.20	-	2.84
Ni-La/ACC(M)	48.28	21.53	13.37	14.32	2.50

According to the BET analysis in Table 2, the specific surface area of the catalysts rises in varying degrees when compared to ACC(M) support. Ni/ACC(M) exhibited the highest specific surface area, most likely owing to the embedded and the adhered nickel particles to the support surface. An interesting aspect was that Ni-La/ACC(M) showed a lower surface area but a greater pore volume and diameter. This may be because the addition of La causes the collapse of some smaller mesopores, resulting in the formation of bigger mesopores in comparison to Ni/ACC(M).

Table 2. Textural parameters of support and catalysts.

Samples	BET Surface Area (m ² ·g ⁻¹)	Pore Volume (cm ³ ·g ⁻¹)	Pore Diameter (nm)
ACC(M)	36.88	0.25	21.35
Ni/ACC(M)	168.09	0.28	7.51
Ni-La/ACC(M)	134.22	0.31	8.34

Furthermore, the N₂ physisorption isotherms of the support and catalysts in Figure 3a showed the IV isotherm and H3 type hysteresis loops, which was due to capillary condensation of the mesoporous, and it displayed a slit-shaped pore [24,25]. The pore diameter distribution curve of catalysts in Figure 3b presented that the catalysts' particle size consisted of many mesopores and a few macropores. Moreover, the existence of mesopores can effectively prevent the aggregation of Ni particles to large particles to prevent premature deactivation of catalysts [26].

**Figure 3.** Adsorption isotherm and particle size distribution of catalysts: (a) Adsorption isotherm; (b) Particle size distribution.

According to SEM/EDS analysis in Figure 4, Ni/ACC(M) showed many irregular lamellar structures that were physically agglomerated, and it created many cavities thus resulting in a high BET surface area. Besides, some mesopores could be detected, which consisted of BET analysis. It was clear that Ni/ACC(M) existed mainly in a rod structure, and Ni-La/ACC(M) existed mainly in the form of a reticular structure. This indicated that the introduction of La resulted in a significant change in the particle size. In terms of

particle size, this is consistent with the conclusion in Mo's study that the size of Ni particles changes with the addition of La_2O_3 [27].

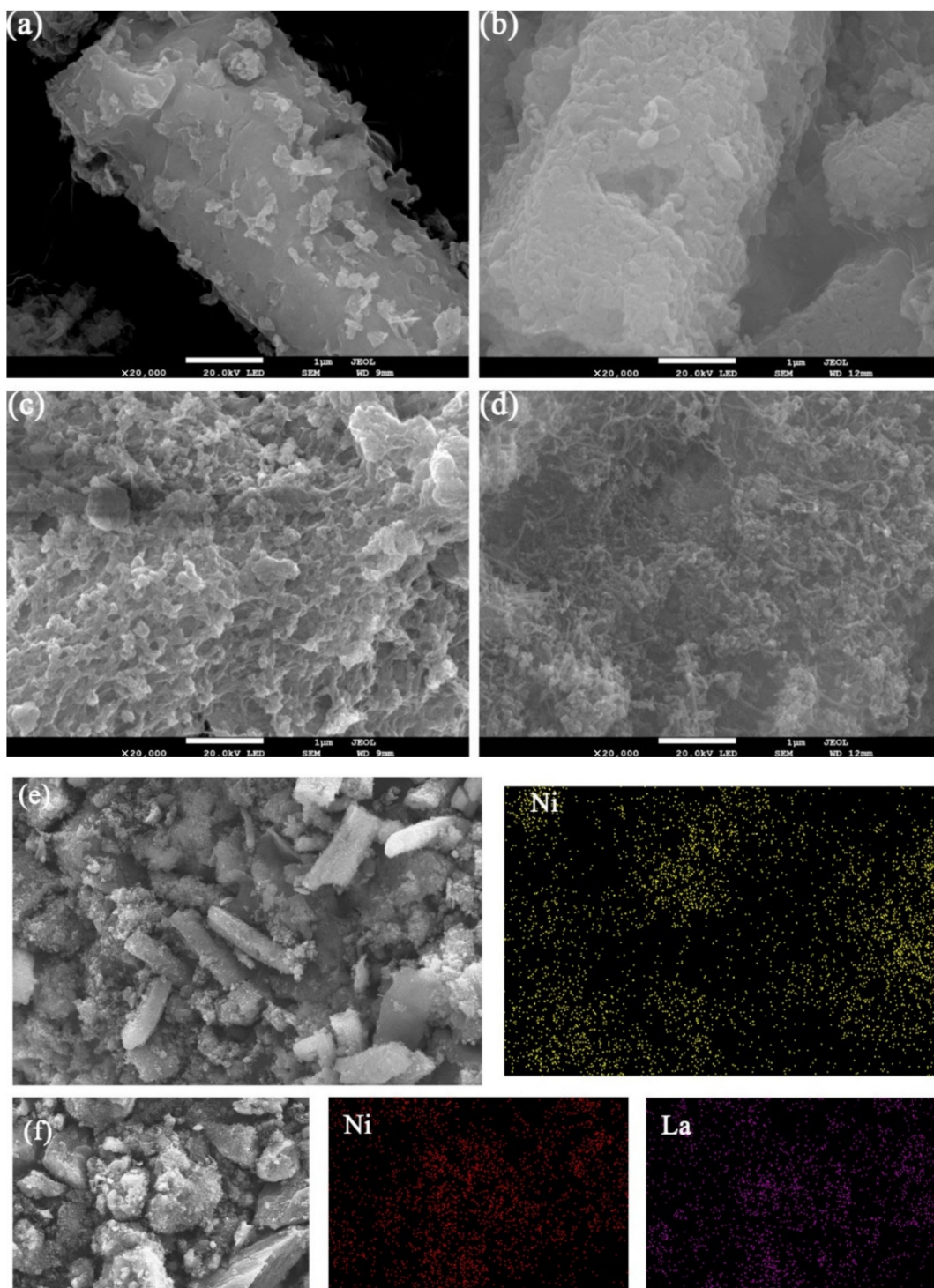


Figure 4. SEM/EDS images of catalysts: (a) fresh Ni/ACC(M); (b) used Ni/ACC(M); (c) fresh Ni-La/ACC(M); (d) used Ni-La/ACC(M); (e) used Ni/ACC(M) mapping; (f) used Ni-La/ACC(M) mapping.

Furthermore, according to Figure 4a,b, the surface of the catalyst produced many irregular blocks after use. Combined with an XRD analysis of NiC_x , it may be carbon deposition on the surface. Figure 4c,d differs from Figure 4a,b in that there are many filamentous carbons instead of blocks. Sakae et al. [28] also found the filamentous carbons

after the reaction of methane decomposing on $\text{Fe}_2\text{O}_3/\text{Al}_2\text{O}_3$ and $\text{Fe}_2\text{O}_3/\text{SiO}_2$ catalysts. Based on the EDS graphs in Figure 4e,f, the active components load successfully, and the addition of La can effectively promote the dispersion of Ni.

2.2. Effect of Raw Material Ratio on Gas Yield

As can be seen from Table 3, the composition and the concentration of the generated gas varied according to the components included in the various raw materials of the catalysts. Without a catalyst, pure soybean straw primarily generated CO , CO_2 , CH_4 , and H_2 , with CO_2 accounting for the higher fraction of 36.33 vol% and H_2 accounting for just 18.91 vol%. In comparison, pure PE generated the majority of CH_4 and H_2 , with CH_4 accounting for 76.29 vol% and H_2 accounting for just 13.06 vol%. The influence of soybean straw and PE ratio on hydrogen generation was investigated to optimize hydrogen production.

Table 3. Proximate and ultimate analysis of Soybean straw and PE.

Samples	Ultimate Analysis (wt%)					Proximate Analysis (wt%)			
	C	H	O*	N	S	M	A	V	FC
Soybean straw	41.08	5.53	52.15	1.24	0.00	4.60	8.70	82.06	4.64
PE	85.78	14.22	-	-	-	-	<0.05	99.95	-

M: Moisture; V: Volatile; A: Ash; FC: Fixed Carbon; O*: by difference; wt%.

The experiments were carried out in the absence of catalysts, with a reaction temperature of 700 °C and a reaction time of 20 min. Figure 5 provides the gas production of raw soybean and PE at different ratios. Neither single soybean straw nor PE has a high percentage of H_2 . The proportion of H_2 gradually increased with the addition of PE. The H_2 content reached a peak when the mass ratio was 5:5, indicating that the co-pyrolysis of straw and PE can promote the decomposition of PE to produce H_2 . This may be due to the fact that straw generates free radical fragments during pyrolysis, and these radicals interact with PE and show synergistic effects in terms of hydrogen production [29]. However, by continuing to add PE, the H_2 content started to decline. The simulated PE pyrolysis mechanism in Liu's study shows that the pyrolysis products of PE contain a variety of complex hydrocarbons and hydrogen [30]. However, in this study, only CH_4 and H_2 can be detected. Hence, the decline of H_2 content is attributed to PE producing a large amount of CH_4 during the pyrolysis process and its content significantly exceeds that of H_2 .

Moreover, it is apparent from Figure 5 that the content of methane increases significantly, and the content of CO_2 decreases gradually until it is zero. This suggests that the yield of H_2 and the hydrocarbons can be improved in the co-pyrolysis of straw with PE, but the production of CO_2 can also be inhibited. The same conclusion was reached in Kai's [10] study. The trend of H_2 content shows that the ratio of soybean straw to PE at 5:5 is the best choice when the maximum H_2 content can be produced.

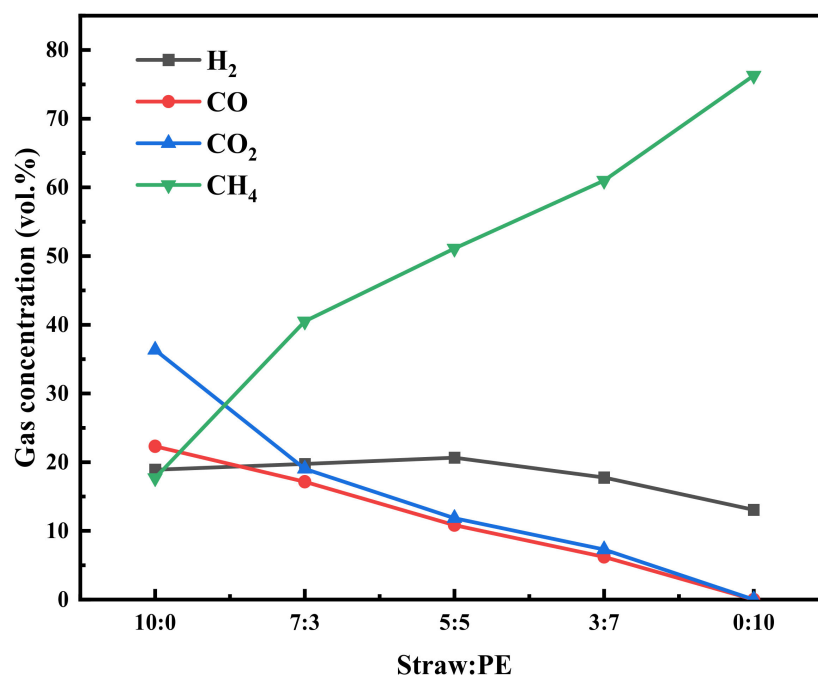


Figure 5. Pyrolysis gas components with different ratios of raw material.

2.3. Effect of Composite Support Ratio on H₂ Yield

Different carriers have a considerable influence on the catalytic performance of Ni-based catalysts. The carrier provides not only mechanical strength but also influences the structure of catalysts and the function of active components [31]. Stronger metal carrier interactions improve the dispersion and the stability of the active component, enhancing the catalyst's performance in pyrolysis. Additionally, the metal-carrier interaction affects the catalyst's reaction activity and selectivity. Conversely, smaller interactions lead to deactivation by the agglomeration of metal species [32,33]. The influence of carrier compounds in various ratios on the gas generation rate during catalytic pyrolysis was examined in this study. In this experiment, the mass ratio of catalyst to feedstock was 1:2, with a reaction temperature of 700 °C and a reaction time of 20 min. In order to obtain more H₂, a straw to PE ratio of 5:5 was used. Figure 6 illustrates the experimental outcomes.

The highest hydrogen generation was 25 vol% less without catalysts, as seen in Figure 7. However, in Figure 6, the H₂ concentration increases to more than 40 vol%, when two different catalysts are used. It shows that these two catalysts can considerably improve H₂ production. Besides, different carrier composite ratios have different effects on the gas. Because of the greater interaction between Ni and the metal carrier of ACC(M) than ACC(W), Ni/ACC(M) is more successful in hydrogen generation. Furthermore, when straw and PE were co-pyrolyzed in the presence of Ni/ACC(M), the H₂ output was 320.6 mL/g, which was 73.30% greater than the 185.0 mL/g obtained by pyrolysis of soybean straw. This is due to a considerable increase in the production of PE gas products, including hydrogen and C₁–C₄ alkanes, after 600 °C pyrolysis [34]. Additionally, this explains the increased content of CH₄ and H₂ in co-pyrolysis. In contrast, the yield of H₂ in co-pyrolysis with Ni/ACC(W) was only 301.2 mL/g, which means that the carrier made better molar ratio at catalyzing.

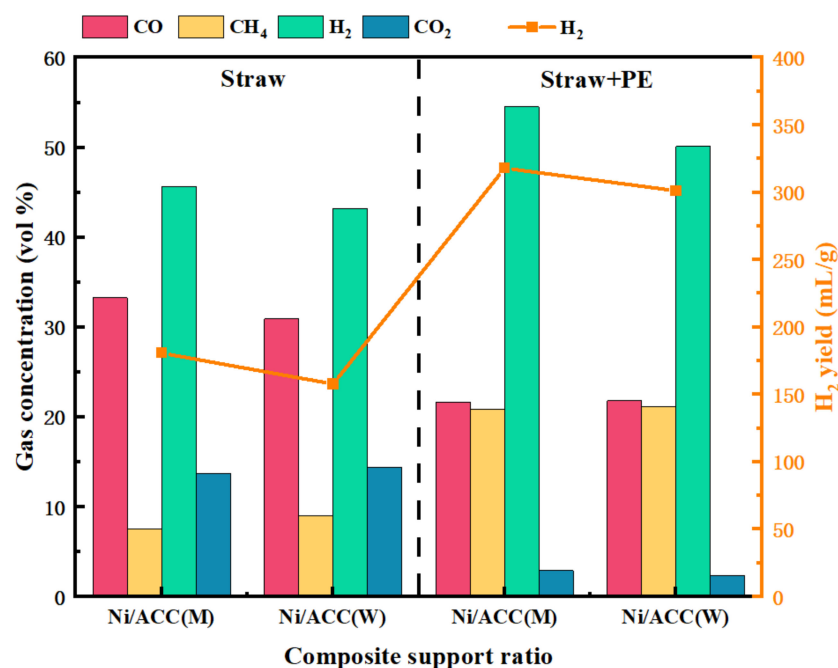


Figure 6. Effect of Ni/ACC support composite ratio on gas production.

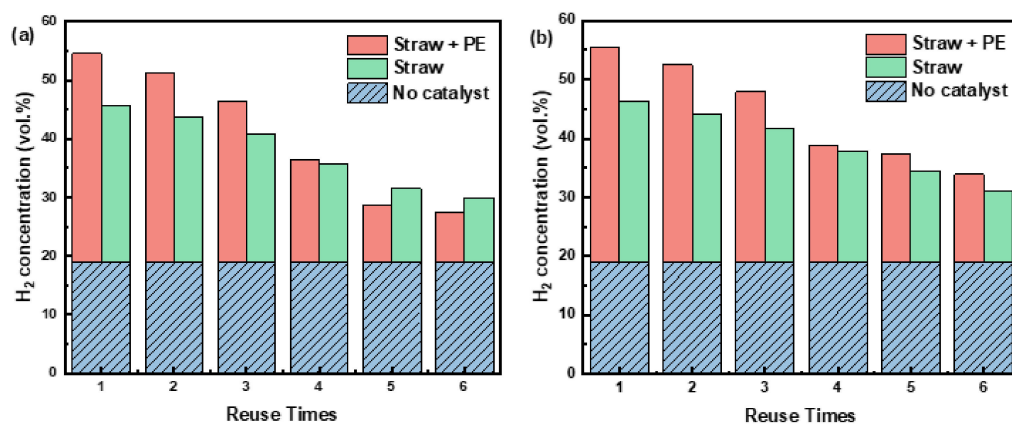


Figure 7. Effect of reuse times of catalysts on hydrogen production: (a) Ni/ACC(M); (b) Ni-La/ACC(M).

2.4. Stability Test of Catalysts

Nickel-based catalysts have been extensively explored in biomass pyrolysis due to their cheap cost and good catalytic efficiency. Single nickel catalysts are prone to deactivation owing to carbon buildup or metal sintering, lowering catalytic efficiency [35]. Various reaction processes alter the structure of activated carbon throughout the pyrolysis process, affecting the catalytic activity [36]. As a result, 10 wt% La was added to the catalyst to increase catalytic activity and stability. The catalyst's stability was determined by gaining 6 times more hydrogen content in the gas product at a reaction temperature of 700 °C and a reaction time of 20 min.

Figure 7 displays the variation of H₂ concentration with the number of uses in the presence of Ni-La/ACC(M) and Ni/ACC(M) catalysts. The findings indicated that the concentration of H₂ produced by both catalysts dropped with increasing their number of use, implying that, on the one hand, Ni's capacity to activate and destroy C-H and C-H declined; on the other hand, the activated carbon matrix in the carrier was destroyed [37]. After the fifth use of Ni/ACC(M) in the pyrolysis of straw or mixes, the H₂ production progressively stabilized. It is worth noting that the volume fraction of H₂ produced by co-pyrolysis was less

than that produced by straw pyrolysis after five applications of the same catalyst, which may be owing to the catalyst's decreased selectivity for H₂. The H₂ content rose by 19.99 mL/g after adding 10 wt% La to the Ni/ACC(M) catalyst for the first time, although the increase was not substantial. However, after five applications, the H₂ content in co-pyrolysis was raised by 24.24 mL/g compared to the Ni/ACC(M) catalyst. This effect might be explained by La improving the interaction between the active component and the carrier, causing the even distribution of the Ni, which can be obtained from SEM/EDS analysis. For calculating used catalysts by Scherrer equation, the crystalline size of nickel was 9.2 nm from the XRD diffraction line corresponding to the Ni (111) plane at 44.5°. However, the La-modification of catalysts significantly changed the crystalline nickel size from 9.2 nm to 5.6 nm, which further proved the influence of uniform Ni distribution by La.

Moreover, after adding La, carbon deposition exists in the form of filamentous carbon rather than massive carbon. Additionally, from the XRD analysis, the sharpness of NiCx peaks is reduced when comparing the catalysts without La. This implies that adding La can not only change the way carbon deposition occurs but may also limit carbon deposition to some extent.

Additionally, after 6 cycles, the H₂ level produced by co-pyrolyzed with Ni-La/ACC(M) catalyst still reached 33.89 vol%. In contrast, Xu et al. [29] produced H₂ by co-pyrolyzing rice husk and PE with Ni/char catalyst. The H₂ content reached only 32 vol% at a 1:1 feedstock ratio, a pyrolysis temperature of 600 °C, a catalytic temperature of 800 °C, and a reaction time of 15 min. These results revealed that the addition of La not only improves catalytic performance but it also improves the catalyst's stability.

3. Experiment

3.1. Chemicals and Materials

Ni(NO₃)₂·6H₂O, La(NO₃)₃·6H₂O, Al(NO₃)₃·9H₂O, Ca(NO₃)₂·4H₂O were obtained from China National Pharmaceutical Group Corporation. NH₃·H₂O and CO(NH₂)₂ (urea) were purchased from Damao Chemical Reagent Factory. The solvent was deionized water in the experiment.

Bamboo and PE were taken from Dongxihu District in Wuhan. Soybean straw came from Datong, Shanxi Province. At first, the bamboo and the soybean straw were cleaned with deionized water and then dried in an oven at 105 °C for 24 h. Afterwards, the processed bamboo and soybean straw were crushed and passed through a 40 mesh sieve. The powdered bamboo and soybean straw were used as biochar and pyrolysis raw materials, respectively. The PE used in the experiment was 40 mesh when purchased.

Biochar was made from powdered bamboo biomass using a tubular furnace having N₂ circulation (L/h). The temperature of the furnace was increased from 20 °C to 800 °C at a heating rate of 10 °C/min. Then, it was kept heated for 2 h with a temperature of 800 °C to obtain bamboo biochar (C).

The proximate and the ultimate compositions of soybean straw and PE were detected in our previous studies [20] (Table 3).

3.2. Catalysts Preparation

Using the homogeneous precipitation method, 10 wt%Ni-10 wt%La/ACC catalysts were synthesized. As a comparison, 10 wt% Ni/ACC catalysts were prepared under the same experimental conditions.

Firstly, ACC carriers were prepared, i.e., Al₂O₃, CaO, and C were compounded into carriers according to the molar ratio and the mass ratio of 1:1:1, respectively. As for molar ratio support, a specific amount of 0.05 mol Al(NO₃)₃·9H₂O and 0.1 mol Ca(NO₃)₂·4H₂O were thoroughly mixed in deionized water with 0.1 mol of the suspended C particles. Subsequently, NH₃·H₂O was added to the previous solution to get a weak alkaline environment, and it was continuously stirred with a magnetic stirrer for 3 h. The solution was left static at room temperature for 6 h and then dried in an oven at 120 °C for 48 h. Finally, the dried material was calcined in a tube furnace at 800 °C for 3 h under continuous N₂ flow conditions, and

the ACC(M) carrier was obtained. The same method was applied to get mass ratio support ACC(W). The composition content of the two carriers is shown in Table 1.

Firstly, $\text{Ni}(\text{NO}_3)_2 \cdot 6\text{H}_2\text{O}$, $\text{La}(\text{NO}_3)_3 \cdot 6\text{H}_2\text{O}$, and $\text{CO}(\text{NH}_2)_2$ (urea) were accurately weighed in deionized water and stirred for 30 min after adding ACC. Then, the sample was heated for 2 h with oil at 115 °C. After that, the sample was left static at room temperature for 6 h. Then, it was treated with deionized water and dried in an oven at 105 °C for 12 h. Finally, it was calcined at 750 °C in a continuous N_2 flow for 2 h. The resulting Ni-La/ACC(W) and Ni-La/ACC(M) catalysts were collected for further analysis.

3.3. Catalysts Characterization

The crystal structure of catalysts was identified by X-ray diffraction (XRD) of Shimadzu XRD-6000 (Kyoto, Japan). The $\text{Cu-K}\alpha$ radiation was applied with the power of 40 kV and 30 mA. The scanning rate and the range were 6°/min and 10~90°, respectively. The metal oxide content of the supported catalysts was measured using an X-ray fluorescence (XRF) device, the Shimadzu EDX-7000. The catalysts were dried thoroughly and evaluated at less than 70% humidity in the room. According to the Brunauer–Emmett–Teller (BET) method, Micromeritics ASAP-2460 was used to test catalysts' surface area, pore volume, and average pore diameter at 77 K and analyzed with N_2 adsorption-desorption isotherms. The catalysts' surface morphology and local chemical composition were determined with JEOL JSM-7100F (Kyoto, Japan), and the accelerating voltage was 20.0 kV by combining the scanning electron microscope (SEM) and the energy dispersive spectroscopy (EDS).

3.4. Experimental Process

The catalytic pyrolysis system is shown in Figure 8. Pyrolysis experiments at the stoichiometric concentration (catalyst:material = 1:2) were performed in a fixed bed reactor (BTF-1200C). Before investigations, nickel-based catalysts supported on ACC and materials were packed in the reactor, built of quartz tubing with a length of 1.4 m and an inner diameter of 60 mm, the reactor was put on the quartz boats under the tube furnace. Furthermore, a steady N_2 flow of 100 mL/min was employed to remove air from the tube furnace to prevent straw and plastic from burning. After purging for 30 min, the reactor was heated to 700 °C at one end of the tube furnace and then the reactor was pushed from one to another, carrying the catalysts and the feedstocks in quartz boats and maintaining the reaction temperature of 700 °C for 20 min. After the reaction, the generated gas was blown out of the tube furnace with N_2 as the inert carrier gas. Finally, the gas was collected using a gas collecting bag, and it was tested using an infrared gas analyzer (Gasboard-3100).

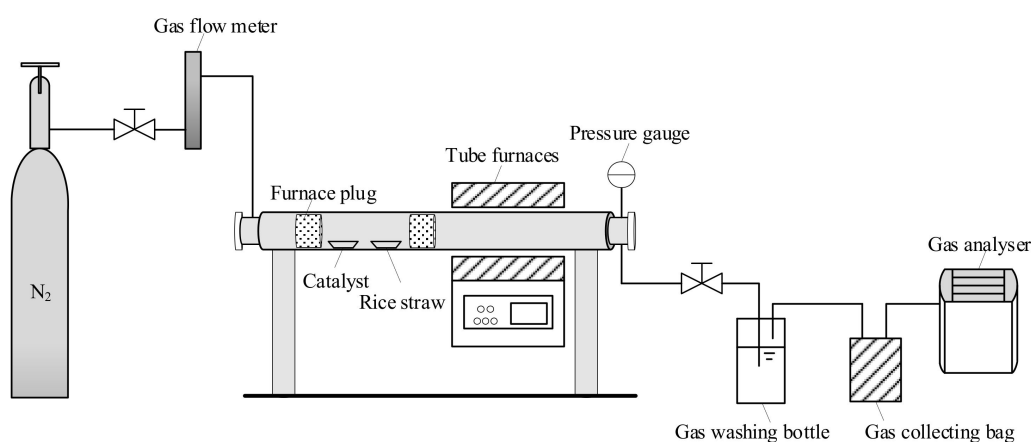


Figure 8. Experimental flow and device diagram.

3.5. Calculation

The concentrations of H₂, CH₄, CO₂, and CO in the product gas (excluding N₂) were analyzed with an infrared gas analyzer. Equation (1) was used for further assessment of the product gas.

$$C_g = \frac{X_g}{X_{H_2} + X_{CH_4} + X_{CO} + X_{CO_2}} \quad (1)$$

where C denotes the yield of gas composition, vol%; X denotes the gas yield from the infrared gas analyzer, vol%.

4. Conclusions

In this work, novel Ni-La/ACC(M) catalysts were produced by a homogeneous precipitation technique for co-pyrolysis of straw and PE for hydrogen generation. The ratio of soybean straw to PE had a substantial effect on the gas concentration, with the best synergy occurring at a mass ratio of 5:5, which resulted in the highest H₂ level. Secondly, the carrier synthesis ratio had an impact. Due to their favorable metal–carrier interactions, carriers compounded in molar ratios were preferred for hydrogen generation. Finally, the addition of La not only increases the H₂ production, but it also significantly extends the catalyst's useful life. In conclusion, at a pyrolysis temperature of 700 °C and a reaction time of 20 min, Ni-La/ACC(M) demonstrated the greatest catalytic effect and stability. The concentration of H₂ reached 55.45 vol% during co-pyrolysis of straw PE, which was 193.23% more than the 18.91 vol% without catalyst, and it was still capable of reaching 33.89 vol% after six uses.

Author Contributions: J.L.: Funding acquisition, Supervision, Writing—Original Draft. R.G.: Writing—Original Draft, Conceptualization, Formal Analysis. L.Z.: Data Curation, Validation. Y.Z.: Data Curation. Z.L.: Resources. B.L.: Investigation. J.W.: Validation. J.H.: Data collection. Y.H.: Supervision, Writing—Review and Editing. Z.Q.: Visualization. M.L.: Writing—Review and Editing. D.G.: Conceptualization, Writing—Review and Editing. All authors have read and agreed to the published version of the manuscript.

Funding: The authors are grateful to “Department of Science and Technology of Hubei Province, Grant No. 2018BEC466,” and “Department of Science and Technology of Hubei Province, Grant No. 2018ZYYD062,” for financial support of the present study.

Data Availability Statement: Not applicable.

Conflicts of Interest: The authors declare no conflict of interest.

References

- bp. bp Statistical Review of World Energy 2021. 2021. Available online: <https://www.bp.com/en/global/corporate/energy-economics/statistical-review-of-world-energy.html> (accessed on 15 October 2021).
- Veziroğlu, T.N.; Şahin, S. 21st Century's energy: Hydrogen energy system. *Energy Convers. Manag.* **2008**, *49*, 1820–1831. [[CrossRef](#)]
- Stefanidis, S.D.; Kalogiannis, K.G.; Iliopoulou, E.F.; Michailof, C.M.; Pilavachi, P.A.; Lappas, A.A. A study of lignocellulosic biomass pyrolysis via the pyrolysis of cellulose, hemicellulose and lignin. *J. Anal. Appl. Pyrolysis* **2014**, *105*, 143–150. [[CrossRef](#)]
- Goyal, H.B.; Seal, D.; Saxena, R.C. Bio-fuels from thermochemical conversion of renewable resources: A review. *Renew. Sustain. Energy Rev.* **2008**, *12*, 504–517. [[CrossRef](#)]
- Cui, B.; Chen, Z.; Wang, F.; Zhang, Z.; Dai, Y.; Guo, D.; Liang, W.; Liu, Y. Facile Synthesis of Magnetic Biochar Derived from Burley Tobacco Stems towards Enhanced Cr(VI) Removal: Performance and Mechanism. *Nanomaterials* **2022**, *12*, 678. [[CrossRef](#)]
- Cui, B.; Chen, Z.; Guo, D.; Liu, Y. Investigations on the pyrolysis of microalgal-bacterial granular sludge: Products, kinetics, and potential mechanisms. *Bioresour. Technol.* **2022**, *349*, 126328. [[CrossRef](#)]
- Jia, Y.; Wang, Y.; Zhang, Q.; Rong, H.; Liu, Y.; Xiao, B.; Guo, D.; Laghari, M.; Ruan, R. Gas-carrying enhances the combustion temperature of the biomass particles. *Energy* **2022**, *239*, 121956. [[CrossRef](#)]
- Hoang, A.T.; Ong, H.C.; Fattah, I.M.R.; Chong, C.T.; Cheng, C.K.; Sakthivel, R.; Ok, Y.S. Progress on the lignocellulosic biomass pyrolysis for biofuel production toward environmental sustainability. *Fuel Process. Technol.* **2021**, *223*, 106997. [[CrossRef](#)]
- Ambursa, M.M.; Juan, J.C.; Yahaya, Y.; Taufiq-Yap, Y.H.; Lin, Y.-C.; Lee, H.V. A review on catalytic hydrodeoxygenation of lignin to transportation fuels by using nickel-based catalysts. *Renew. Sustain. Energy Rev.* **2021**, *138*, 110667. [[CrossRef](#)]
- Kai, X.; Li, R.; Yang, T.; Shen, S.; Ji, Q.; Zhang, T. Study on the co-pyrolysis of rice straw and high density polyethylene blends using TG-FTIR-MS. *Energy Convers. Manag.* **2017**, *146*, 20–33. [[CrossRef](#)]

11. Fan, H.; Gu, J.; Hu, S.; Yuan, H.; Chen, Y. Co-pyrolysis and co-gasification of biomass and polyethylene: Thermal behaviors, volatile products and characteristics of their residues. *J. Energy Inst.* **2019**, *92*, 1926–1935. [[CrossRef](#)]
12. Yang, T.; Hu, K.; Li, R.; Sun, Y.; Kai, X. Cogasification of typical plastics and rice straw with carbon dioxide. *Environ. Prog. Sustain. Energy* **2015**, *34*, 789–794. [[CrossRef](#)]
13. Sajdak, M. Impact of plastic blends on the product yield from co-pyrolysis of lignin-rich materials. *J. Anal. Appl. Pyrolysis* **2017**, *124*, 415–425. [[CrossRef](#)]
14. Zhang, S.; Zhu, S.; Zhang, H.; Liu, X.; Xiong, Y. High quality H₂-rich syngas production from pyrolysis-gasification of biomass and plastic wastes by Ni-Fe@Nanofibers/Porous carbon catalyst. *Int. J. Hydrogen Energy* **2019**, *44*, 26193–26203. [[CrossRef](#)]
15. Chai, Y.; Wang, M.; Gao, N.; Duan, Y.; Li, J. Experimental study on pyrolysis/gasification of biomass and plastics for H₂ production under new dual-support catalyst. *Chem. Eng. J.* **2020**, *396*, 125260. [[CrossRef](#)]
16. Guo, D.; Hu, M.; Chen, Z.; Cui, B.; Zhang, Q.; Liu, Y.; Luo, S.; Ruan, R.; Liu, Y. Catalytic pyrolysis of rain tree biomass with nano nickel oxide synthesized from nickel plating slag: A green path for treating waste by waste. *Bioresour. Technol.* **2020**, *315*, 123831. [[CrossRef](#)]
17. Gao, N.; Salisu, J.; Quan, C.; Williams, P. Modified nickel-based catalysts for improved steam reforming of biomass tar: A critical review. *Renew. Sustain. Energy Rev.* **2021**, *145*, 111023. [[CrossRef](#)]
18. Chan, F.L.; Tanksale, A. Review of recent developments in Ni-based catalysts for biomass gasification. *Renew. Sustain. Energy Rev.* **2014**, *38*, 428–438. [[CrossRef](#)]
19. Cui, X.; Ren, P.; Deng, D.; Deng, J.; Bao, X. Single layer graphene encapsulating non-precious metals as high-performance electrocatalysts for water oxidation. *Energy Environ. Sci.* **2016**, *9*, 123–129. [[CrossRef](#)]
20. Zhang, Y.; Li, J.; Li, B.; Li, Z.; He, Y.; Qin, Z.; Gao, R. Preparation of Ni-La/Al₂O₃-CeO₂-Bamboo Charcoal Catalyst and Its Application in Co-pyrolysis of Straw and Plastic for Hydrogen Production. *BioEnergy Res.* **2021**, 1–14. [[CrossRef](#)]
21. Manera, C.; Perondi, D.; Barcellos, T.; Godinho, M. CO₂ gasification of elephant grass: Effect of Ni/mayenite catalyst on dry reforming of tar. *Biomass Bioenergy* **2020**, *143*, 105829. [[CrossRef](#)]
22. He, Z.; Wang, X.; Liu, R.; Gao, S.; Xiao, T. Performances of different additives on NiO/γ-Al₂O₃ catalyst in CO methanation. *Appl. Petrochem. Res.* **2016**, *6*, 235–241. [[CrossRef](#)]
23. Jurado, L.; Papaefthimiou, V.; Thomas, S.; Roger, A.-C. Upgrading syngas from wood gasification through steam reforming of tars over highly active Ni-perovskite catalysts at relatively low temperature. *Appl. Catal. B Environ.* **2021**, *299*, 120687. [[CrossRef](#)]
24. Lee, H.-S.; Lee, J.; Seo, H.; Kang, H.; Kim, D.H.; Lee, Y.-W. Evaluation of Pd/ZSM-5 catalyst for simultaneous reaction of transesterification and partial catalytic transfer hydrogenation of soybean oil under supercritical methanol. *Fuel Process. Technol.* **2021**, *218*, 106870. [[CrossRef](#)]
25. Ren, J.; Liu, Y.-L. Boosting syngas production from corncob tar reforming over Ni/MgAl hydrotalcite-derived catalysts. *Fuel* **2022**, *307*, 121779. [[CrossRef](#)]
26. Ma, H.; Zeng, L.; Tian, H.; Li, D.; Wang, X.; Li, X.; Gong, J. Efficient hydrogen production from ethanol steam reforming over La-modified ordered mesoporous Ni-based catalysts. *Appl. Catal. B Environ.* **2016**, *181*, 321–331. [[CrossRef](#)]
27. Mo, W.; Ma, F.; Ma, Y.; Fan, X. The optimization of Ni-Al₂O₃ catalyst with the addition of La₂O₃ for CO₂-CH₄ reforming to produce syngas. *Int. J. Hydrogen Energy* **2019**, *44*, 24510–24524. [[CrossRef](#)]
28. Takenaka, S.; Serizawa, M.; Otsuka, K. Formation of filamentous carbons over supported Fe catalysts through methane decomposition. *J. Catal.* **2004**, *222*, 520–531. [[CrossRef](#)]
29. Xu, D.; Xiong, Y.; Zhang, S.; Su, Y. The synergistic mechanism between coke depositions and gas for H₂ production from co-pyrolysis of biomass and plastic wastes via char supported catalyst. *Waste Manag.* **2021**, *121*, 23–32. [[CrossRef](#)]
30. Liu, X.; Li, X.; Liu, J.; Wang, Z.; Kong, B.; Gong, X.; Yang, X.; Lin, W.; Guo, L. Study of high density polyethylene (HDPE) pyrolysis with reactive molecular dynamics. *Polym. Degrad. Stab.* **2014**, *104*, 62–70. [[CrossRef](#)]
31. Zhang, G.; Liu, J.; Xu, Y.; Sun, Y. A review of CH₄-CO₂ reforming to synthesis gas over Ni-based catalysts in recent years (2010–2017). *Int. J. Hydrogen Energy* **2018**, *43*, 15030–15054. [[CrossRef](#)]
32. Tathod, A.P.; Hayek, N.; Shpasser, D.; Simakov, D.S.A.; Gazit, O.M. Mediating interaction strength between nickel and zirconia using a mixed oxide nanosheets interlayer for methane dry reforming. *Appl. Catal. B Environ.* **2019**, *249*, 106–115. [[CrossRef](#)]
33. Zhang, R.-J.; Xia, G.-F.; Li, M.-F.; Wu, Y.; Nie, H.; Li, D.-D. Effect of support on the performance of Ni-based catalyst in methane dry reforming. *J. Fuel Chem. Technol.* **2015**, *43*, 1359–1365. [[CrossRef](#)]
34. Zhao, D.; Wang, X.; Miller, J.B.; Huber, G.W. The Chemistry and Kinetics of Polyethylene Pyrolysis: A Process to Produce Fuels and Chemicals. *ChemSusChem* **2020**, *13*, 1764–1774. [[CrossRef](#)] [[PubMed](#)]
35. Gao, X.; Ashok, J.; Kawi, S. Smart Designs of Anti-Coking and Anti-Sintering Ni-Based Catalysts for Dry Reforming of Methane: A Recent Review. *Reactions* **2020**, *1*, 13. [[CrossRef](#)]
36. Liang, S.; Guo, F.; Du, S.; Tian, B.; Dong, Y.; Jia, X.; Qian, L. Synthesis of Sargassum char-supported Ni-Fe nanoparticles and its application in tar cracking during biomass pyrolysis. *Fuel* **2020**, *275*, 117923. [[CrossRef](#)]
37. Hu, J.; Jia, Z.; Zhao, S.; Wang, W.; Zhang, Q.; Liu, R.; Huang, Z. Activated char supported Fe-Ni catalyst for syngas production from catalytic gasification of pine wood. *Bioresour. Technol.* **2021**, *340*, 125600. [[CrossRef](#)]